Observation of photoinduced carrier dynamics at the interface by means of time-resolved hard X-ray photoelectron spectroscopy

Masaki Oura (oura@spring8.or.jp)
Soft X-ray Spectroscopy Instrumentation Unit, and also
SR Materials Science Instrumentation Unit
Research Infrastructure Group, Advanced Photon Technology Division,
RIKEN SPring-8 Center

Hitoshi Osawa (hitoshio@spring8.or.jp)
Advanced Nano Measurement Support Team
Nanotechnology Research Promotion Group
Japan Synchrotron Radiation Research Institute (JASRI)

ABSTRACT :

It is well known that hard X-ray photoelectron spectroscopy (HAXPES) is one of the most powerful methods to investigate the bulk electronic structure of condensed matter. In order to extend its capability for studying transient electronic states in the time-scale from femtosecond to subnanosecond regimes, we have been developing a time-resolved HAXPES system at the ultra-short high-brilliance X-ray sources, such as the 27m-long undulator beamline BL19LXU of SPring-8 and the X-ray free electron laser facility SACLA.

In the practical course, participants will learn the principle of HAXPES and measure the core-level photoelectron as well as Auger electron spectra of target material. Furthermore, with the use of femtosecond optical laser and also the X-ray chopper, we will try to perform the observation of photoinduced carrier dynamics at SiO_2/Si interface by time-resolved HAXPES. Participants will also learn how we can realize time-resolved HAXPES to study the ultrafast dynamics of electronic structure in condensed matter.

1. Introduction

1.1 Photoelectron Spectroscopy (PES)

Photoelectron Spectroscopy (PES) is one of the most important techniques to study the electronic structure of materials [1]. The electronic structure of a material describes the energies of electrons in a material. The energy of electrons in an isolated atom get modified when the atoms get arranged into a solid or a liquid, or even a gaseous molecule, but they can still be described in terms of their energy levels in an atom. The type of electrons (*s, p, d, f*), the number of a particular type of electron in an atom, and the energy the electrons possess in a material, determine the chemical and physical properties of a

material. For example, the energy distribution of electrons of a particular atom existing in an insulator (such as copper atoms in cupric oxide, CuO) and in a metal (such as copper atoms in copper) are different, although they originate from the same type of atoms, namely, copper atoms. This difference in energy distribution is directly related to the valency of copper in copper metal (Cu^0) as compared to its valency in insulating cupric oxide (Cu^{2+}). The electronic energy levels of a material can also depend on very small amount of changes in its chemical composition. This is appropriately described by the change in properties of an intrinsic semiconductor obtained upon doping very small amount of holes and electrons by chemical substitution. The best example is p-type (hole) or n-type (electron) doping in silicon achieved by site-substitution of boron or phosphorus atoms, respectively. The precise control of doping holes and electrons in various semiconductors such as Si, Ge, GaAs, GaN, *etc*. is the basis of manufacturing a variety of electronic devices, from rectifier diodes and light emitting diodes (LEDs) to state of the art integrated circuits (ICs) like microprocessors, memory chips, *etc*. Another important topic in materials science is phase transitions : a material can undergo a transformation in its geometric structure and/or properties as a function of a physical parameter such as temperature, pressure, *etc*. The competition in the elastic energy of a material versus its electronic energy often leads to a phase transition as a function of a physical parameter. Accordingly, the elucidation of the electron energies of a material is a major field of study in present day research.

1.2 Salient Features of PES

PES is a primary tool to study the electronic structure of materials – solid, liquid or gas. It has been used to study the electronic structure of solids extensively over the last 50 years and today, there exists a large database of the electronic structure of materials as determined by photoelectron spectroscopy. The earliest record of experiments describing photoelectrons (that is, photon induced emission of electrons, also called photoemission) is due to the German physicist, Heinrich Hertz (1856–1894) as part of his studies on the nature of electro-magnetic radiation and the experimental discovery of the photoelectric effect [2]. From a series of experiments, Hertz showed that the absorption of electro-magnetic radiation (=photon) by a material placed near a spark gap, directly affected the current-voltage (=electric) characteristics of a spark gap : the first illustration of photo-electric effect. Since the flow of current across a spark gap is due to electrons, it meant that the electro-magnetic radiation affected the electrons in the material. Historically, these experiments were done before the discovery of the electron by J. J. Thomson in 1899 and the photoelectric effect experiments could not be reconciled with the classical or wave nature of electro-magnetic radiation. It was later explained by Albert Einstein [3], based on the quantum nature of electro-magnetic radiation, which describes light (electro-magnetic radiation) as consisting of photons and every photon has a specific frequency ν and energy $h\nu$. The Nobel Prize citation of Albert Einstein reads “for his services to the

development of Theoretical Physics, and especially for his discovery of the law of the photoelectric effect". The photoelectric effect is described by the equation,

$$h\nu = KE + BE + \Phi \qquad (1)$$

where, hν is the known incident photon energy, KE ($=E_K$) is the measured kinetic energy of the emitted electron, BE ($=E_B$) is the binding energy of the electron, and Φ is the known work function of the material under study. This equation tells us that if the incident photon energy is more than the sum of the binding energy of an electron and the work function of a material, on absorbing the photon, the electron will get emitted with a finite kinetic energy. The important features of the photoelectric effect are :

(1) The rate at which electrons are emitted is directly proportional to the intensity of the incident light, for a given material and frequency of incident radiation.

(2) For every material, there exists a certain minimum frequency of incident radiation below which electrons cannot be emitted by the photoelectric effect, and this minimum frequency is called the threshold frequency.

(3) For incident radiation above the threshold frequency, the maximum kinetic energy of the emitted electron depends on the frequency of incident radiation, but not on the intensity of the incident radiation.

These features were a direct proof of the particle nature of electro-magnetic radiation and played a vital role in establishing the wave-particle duality principle in quantum mechanics. The equation (1) above is a statement of the law of conservation of energy and implicitly includes the law of conservation of momentum.

1.3 Technique of PES

The photoelectron "spectroscopy" experiment involves measuring the intensity of photo-emitted electrons from the core levels and valence band of a material, as a function of kinetic energy of the emitted electrons. Figure 1 shows a schematic of the photoelectron process.

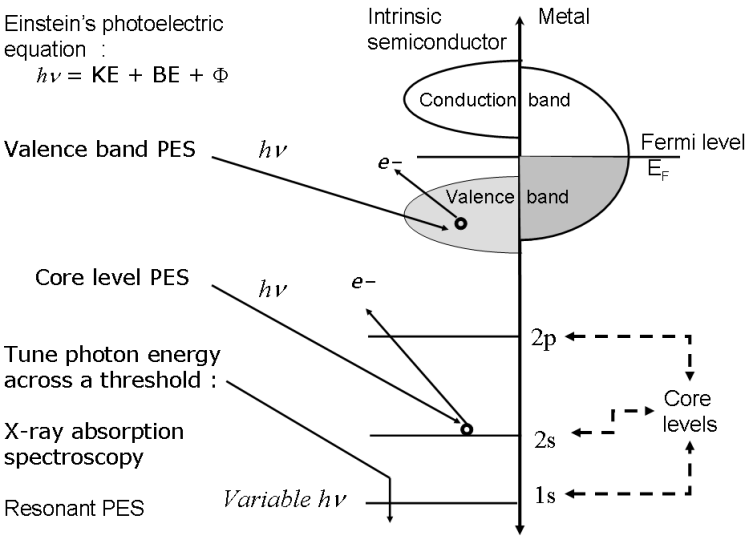

Figure 1. A schematic diagram showing the energy ofelectrons in a material and the process of the photoelectric effect.

Pioneering work on the science and technique of photoelectron spectroscopy for the study of electronic structure [4], or "ESCA" (an acronym for electron spectroscopy for chemical analysis), was carried out by the group of Kai Siegbahn (1918–2007) at

Uppsala University in Sweden. He was awarded the Nobel Prize for "his contribution to the development of high-resolution electron spectroscopy" in 1981. The schematic of the instrumentation required for carrying out photoelectron spectroscopy is shown in Fig. 2. Since we have to measure electron kinetic energy, the experiment has to be done in ultra high vacuum (UHV), because electrons have a very short mean free path in air [5,6]. Typically, one needs a vacuum of better than 10^{-6} mbar (= 10^{-4} Pascal), in the case of experiment for materials science, it is typically in the range of 10^{-8} Pa. Further, the electrons also have a short inelastic mean free path inside a solid [5-7]. The inelastic mean free path (IMFP) of an electron inside a solid is defined as the average distance travelled by an electron before making an inelastic collision. Since an inelastic collision results in a change of its energy, it leads to a loss of the signal intensity that is being measured. So the technique can be extremely surface sensitive and probes typically a few angstroms to about 20Å of the surface with conventional laboratory equipment of the type shown in Figure 2.

For a material with an IMFP, λ, the measured intensity I is given by,

$$I = I_o \exp(-d/\lambda) \qquad (2)$$

where, I_o is the intensity without any inelastic losses and d is the distance from the surface from which the electrons are emitted. The IMFP λ depends strongly on the kinetic energy of the electrons, and also the specific properties of the material under investigation. However, a general empirical curve, well-known as the universal curve for IMFP of electrons [5,6], shows that the IMFP has large values ($> 50-100$ Å) for very low kinetic energies (< 10 eV), a broad minimum of $5-10$ Å for kinetic energies between $30-100$ eV, and then a monotonic increase for kinetic energies above 100 eV. Typically, the IMFP is again about $50-150$ Å at energies of $6-8$ keV. The surface sensitivity is thus determined by the depth perpendicular to the surface from which the electrons escape, and is defined as the mean escape depth $\sigma = \lambda \cos\alpha$, where λ is the IMFP and α is the emission angle of the electrons measured with respect to the surface normal. The technique is thus most bulk sensitive at normal emission, and as the emission angle increases, it becomes more surface sensitive.

The general photoelectron spectroscopy instrument consists of stainless steel chambers which are pumped by a combination of UHV turbo-pumps, backed by rotary/diaphragm pumps. A typical stand-alone instrument (Figure 2) consists of three chambers : (1) a main chamber, *i.e.* analysis chamber, has an electron energy analyzer and a sample manipulator which usually facilitates sample cooling and heating, (2) a preparation chamber in which the sample surface is prepared and characterized inside the UHV (this chamber usually has a sample cleaver or, sample annealing and ion-etching facilities, *etc.*) and (3) a fast entry load-lock or sample bank chamber, which alone is opened and exposed to air, for introducing the samples into the preparation and analysis chambers. This load-lock chamber is necessary for minimizing the time required to achieve UHV condition for experiments to be done in the preparation and analysis chambers. As is shown in Figure 2,

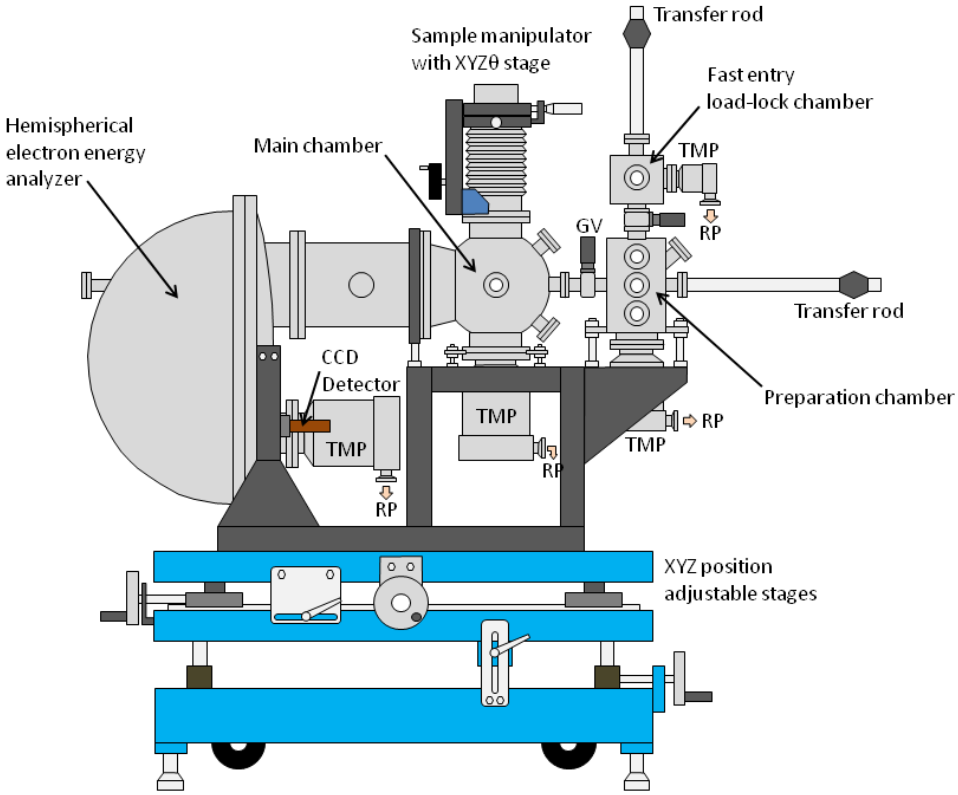

Figure 2. Schematic of a photoelectron spectrometer equipped with various components. TMP : Turbomolecular Pump, RP : Rough Pump, GV : Gate Valve

the photoelectron spectroscopy experiments usually use a hemispherical electron energy analyzer for measuring the kinetic energies of electrons, which is achieved by applying a fixed voltage to the hemispherical plates of the analyzer for one particular kinetic energy. The energy analysis is computer controlled and the spectroscopy experiment scans over the kinetic energy of the measured electrons to obtain a spectrum: intensity as a function of kinetic energy. The spectrum can be readily presented as a function of binding energy by knowing the work function or calibrating the energy scale with a standard database of core-level energies [8]. Photoelectron spectroscopy is often done using a fixed photon energy, but it can be done with a photon energy of a few eV (*e.g.* 6 or 7 eV) or even with several keV (*e.g.* 6 or 8 keV). It is also done as a function of tunable photon energy obtained from a synchrotron in the special case of resonant photoelectron spectroscopy.

1.4 Nomenclature

The following table lists the various names and acronyms used in the literature for photoelectron spectroscopy, depending on the energy of photons used for the experiment. Also listed are names and acronyms of the complementary techniques of electron spectroscopy :

Photon energy	Name	Acronym
Ultraviolet (UV) photons : He I (21.2 eV), He II (40.8 eV)	Ultraviolet Photoelectron Spectroscopy	UVPES or UPS
Laboratory X-rays : Mg Kα (1253.6 eV), Al Kα (1486.6 eV)	X-ray Photoelectron Spectroscopy	XPS
Lasers : 4th harmonic of Ti-sapphire laser (5.95 eV), frequency-tripled Nd:YVO_4 laser (6.99 eV)	Laser Photoelectron Spectroscopy	Laser-PES
Tunable UV and soft X-ray photons (30 – 1500 eV) using grating monochromators at a synchrotron	Resonant Photoelectron Spectroscopy	Resonant-PES
Hard X-rays obtained at a synchrotron using crystal monochromators (6 – 10 keV)	Hard X-ray Photoelectron Spectroscopy	HAXPES

Complementary techniques :	
Inverse photoelectron spectroscopy	IPES
Bremsstrahlung isochromat spectroscopy	BIS
X-ray Absorption spectroscopy	XAS

A further classification involves the names/nomenclature used to describe specific energy levels that are measured in a material, as known from the energy levels of the electronic states present in the atoms constituting the material. The nomenclature follows the well-known classification for hydrogenic atoms such as *s, p, d, f* electrons occupying the K, L, M, N, *etc*. shells in an atom [9]. The table below lists a more detailed classification for electron energy levels from the K-shell to N-shell :

K-shell	$1s^2$	K
L-shell	$2s^2$ $2p^6$: $2p_{1/2}$, $2p_{3/2}$	L_1 L_2, L_3
M-shell	$3s^2$ $3p^6$: $3p_{1/2}$, $3p_{3/2}$ $3d^{10}$: $3d_{3/2}$, $3d_{5/2}$	M_1 M_2, M_3 M_4, M_5
N-shell	$4s^2$ $4p^6$: $4p_{1/2}$, $4p_{3/2}$ $4d^{10}$: $4d_{3/2}$, $4d_{5/2}$ $4f^{14}$: $4f_{5/2}$, $4f_{7/2}$	N_1 N_2, N_3 N_4, N_5 N_6, N_7

The above classification is fully described in references 5 and 9. Photoelectron spec-

troscopy measures the occupied electronic states of a material and describes the core (or inner)-levels and valence (outermost) levels of a material. A related technique to photoelectron spectroscopy is Auger electron spectroscopy [1,5,6]. When an electron is emitted from a core level, it results in an excited state with a core hole. This hole can get filled by a higher lying electron and the energy of this transition is given out in the form of a photon (resulting in X-ray emission), or the excess energy can be used in a non-radiative process to remove another electron. The second process, which results in the emission of an electron is called the Auger effect, thus giving the name Auger electron spectroscopy. Later, we will discuss three related or complementary electron spectroscopies of the unoccupied and occupied electron states of a material, which go by the names of inverse photoelectron spectroscopy [10], X-ray absorption spectroscopy [11], resonant photo-electron spectroscopy [12], respectively. The method of inverse photoelectron spec-troscopy (IPES) is a valuable probe of the unoccupied density of states of a material, based on the inverse process of photoelectric effect [12] *i.e.* absorption of an electron and emission of a photon. However, it is a very time consuming experiment and is not very popular because the intensities are very low due to the low transition probability for the inverse photoelectric process. The experiments of X-ray absorption spectroscopy and resonant photoelectron spectroscopy require comparatively very little time, but require a tunability of the incident photon energies.

1.5 Applications

In the following, we describe the major applications of photoelectron spectroscopy.

1.5.1 Core-level photoelectron spectroscopy

Since atoms of each element possess a unique set of electron energy levels, the foremost application of photoelectron spectroscopy is to identify the elements present in a material, from a measurement of its core level spectra. Using tabulated atomic sensitivity factors S_i for specific core levels (or atomic cross-sections) [13], one can also quantify the ratio of elements present in a sample by measuring the core-level spectra of the different elements present in a sample. The atomic fraction F_β of a constituent element β in a sample is given by,

$$F_\beta = (I_\beta/S_\beta) / \Sigma (I_i/S_i) \qquad (3)$$

where, the sum is over a specific core level of each element *i* present in the sample and I_i are their respective intensities.

1.5.2 Identification of chemical or valence state

The chemical state of an element can be determined because the core-level binding energies of elements depends on their valency. *e.g.* it is a routine experiment to identify and distinguish [8] a metal and its oxide such as aluminum metal (Al^0) and aluminum (Al^{3+}) oxide, or copper metal (Cu^0) and cupric (Cu^{2+}) oxide. In more complex situations, it is possible to distinguish between multiple oxidation states using core-level spectroscopy.

This is best exemplified by Si 2p core-level spectra which showed that features due to Si^0 (elemental Silicon), Si^{1+}, Si^{2+}, Si^{3+} and Si^{4+} are systematically shifted to higher binding energies, depending on the valence state [14]. A schematic figure is shown in Figure 3, plotted as a function of relative binding energy. The absolute binding energy for elemental silicon 2p core level is about 99 eV, and every higher multiple oxidation state is about 1 eV higher binding energy, with the Si^{4+} occurring at about 103 eV. Thus, even suboxides can be identified and quantified using photoelectron spectroscopy and lead to a description of local bonding configurations in materials. At a general level, core-level photoelectron spectroscopy applications in surface science involve the determination of physisorption or chemisorption of molecules, as determined from the binding energies and symmetry of molecules adsorbed on surfaces.

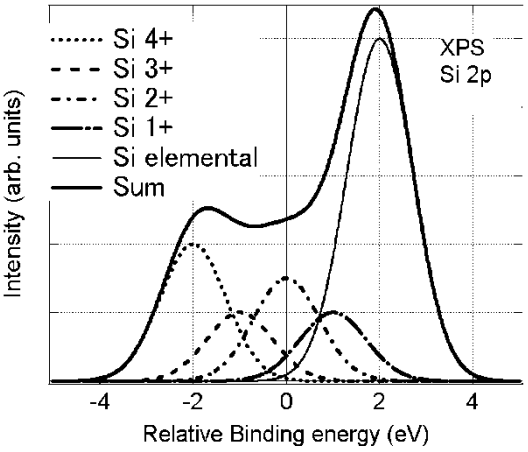

Figure 3. Schematic showing multiple oxidation states of silicon, as measured in Si 2p core-levels as measured from an oxidized Silicon surface, using X-ray photoelectron spectroscopy.

1.5.3 Line shape analysis

A detailed study of core-level lineshapes using high energy resolution can reveal material properties : a symmetric line shape for insulators, or an asymmetric line shape for metals. The symmetric lineshape (Figure 4) is described by a Voigt function : a convolution of a Gaussian function (representing the experimental energy resolution) with a Lorentzian function (representing the lifetime of the energy level). The lifetime (Δt) of a specific core level is related to the intrinsic energy width (ΔE) of the core level reflecting the Heisenberg's uncertainty principle, and is given by, $\Delta E \cdot \Delta t \geqq \hbar$; $\hbar = h/2\pi$ where h is the Planck's constant.

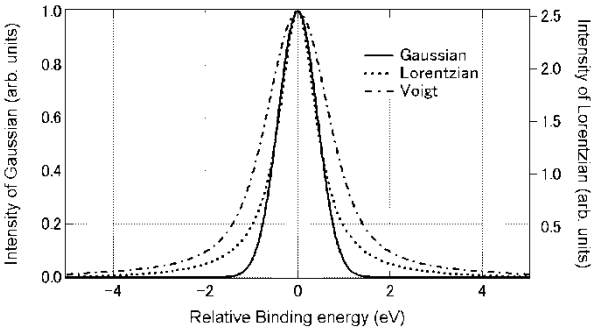

Figure 4. Comparison of a Gaussian function (dashed line) and Lorentzian function (dotted line) of the same full width at half maximum (FWHM = 1 eV), and its convolution, a Voigt function (dash-dot line).

Metals show an asymmetric line- shape that is well-described by a Doniach-Sunjic line shape [15], which is due to the excitations of electron-hole pairs at the Fermi level of a

metal. Since these electron-hole excitations have infinitesimally small energies and occur when the electron is travelling within the solid, they result in a loss of kinetic energy of the emitted electron. This loss in kinetic energy causes a broadening on the low kinetic energy (high binding energy) side of an otherwise symmetric core level, and is a characteristic of metals. Core-level lineshapes also carry valence electron spin information. The splitting of the 3s core levels in a molecular gas is indicative of the exchange coupling between the s core levels and the valence electron spin [4] *e.g.* the oxygen 1s core-level spectrum of molecular oxygen consists of two peaks separated by 1.1 eV and with an intensity ratio of 1:3 which is proportional to the degeneracy of the states. This behaviour is understood as follows : The photoelectron of one 1s electron results in a photohole with a spin of s = 1/2. Since molecular oxygen has a total valence electron spin of S = 1, it couples with the s = 1/2 spin and gives a total spin J = 1/2 and 3/2. The degeneracy is given by 2J+1 and hence the intensities are in the ratio of 1:3. Water, with a valence electron spin of S = 0 does not show this exchange splitting in the O 1s core-level spectrum. Similar behaviour is also known in the 3s, 4s and 5s core-level spectra of transition metal and rare-earth compounds [1].

1.5.4 Valence band photoelectron spectroscopy

A direct probe of the occupied density of states (DOS, number of electronic states, which is proportional to the measured intensity of electronic states as a function of their energy) of a material is provided by valence band photoelectron spectroscopy. Thus, one can distinguish between an intrinsic semiconductor (or insulator) compared to a metal, because semiconductors (or insulators) have a gap in the density of states at the chemical potential, or Fermi level E_F, while a metal has no gap in the density of states (See Figure 1). The Fermi level of a metal (the highest occupied energy level of a metal) is identified as the highest kinetic energy level that can be measured using a specific photon energy and is called the Fermi edge. At zero temperature, it is a sharp cut-off or step-function as determined by the Fermi-Dirac distribution function but since any experiment is done at a finite temperature, the Fermi level is broadened at the edge by the Fermi-Dirac function at that temperature. The Fermi edge is often used to determine the energy resolution of a photoelectron spectrometer, defined as the Gaussian function that needs to be convoluted with the Fermi-Dirac function (Figure 5), which simulates the Fermi edge spectrum accurately at the temperature of the measurement.

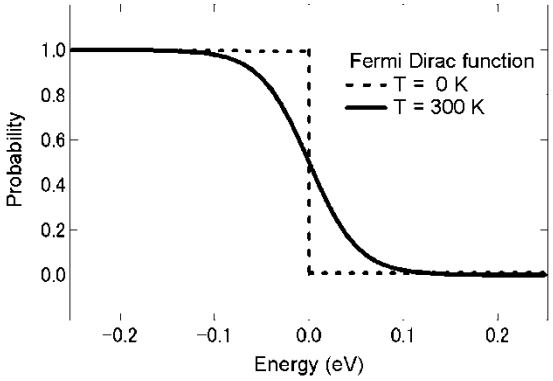

Figure 5. The Fermi-Dirac function at T = 0 and 300 K. Note x-scale is in eV

The present record for energy resolution in photoelectron spectroscopy of a solid is 360 micro-electron volts (μeV), obtained for the Fermi edge of gold measured at a temperature of 3 K, using a laser as a photon source [16] (Figure 6). A high energy resolution of about 1–5 meV has been achieved by several groups in the world in the past few years. High energy resolution photoelectron spectroscopy has played a very important

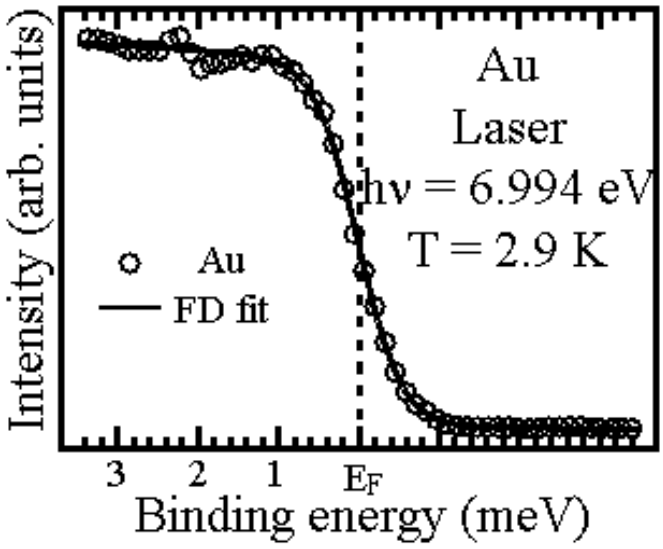

Figure 6. The highest energy resolution photoelectron spectrum (*circles*) of gold (Au), measured for a solid using Laser PES at a sample temperature of 2.9 K, compared with a FD fit (*full line*), a Fermi-Dirac function convoluted with a Gaussian function having a full width at half maximum of 360 micro-eV. Note x-scale is in milli-eV (from Ref. 16).

role in the study of phase transitions including superconductivity, metal-insulator transitions, Kondo materials, *etc*. and defines the frontline of research in the electronic structure of novel materials.

1.5.5 Angle-resolved photoelectron spectroscopy

In angle-resolved photoelectron spectroscopy (ARPES) experiments, in addition to measuring the kinetic energies of the emitted electrons, one measures the spectra as a function of emission angle with respect to the surface normal, in terms of the polar and azimuth angles. Before we describe the ARPES technique, it is useful to consider the photoemission process as involving the initial state with energy, $E_i = -BE$ (negative of the binding energy of the electron) and the final state of the electron after emission as a state with an energy $E_f = KE + \Phi$. This implies $E_f = E_i + h\nu$, from the photoelectric equation. Applying the law of conservation of momentum to the electrons in a crystalline solid with initial state energy and momentum as (E_i,k_i) and the final state to be described by (E_f,k_f),

the electron emitted from the solid has the measured momentum $K_f = k_f + G$ where G is a reciprocal lattice vector. Under the assumption of a free electron final state, with k_f resolved into the in-plane momentum $k_\parallel$ and out of plane momentum $k_\perp$, the KE of emitted electron is

$$E_K = (\hbar^2 / 2m)(k_\parallel^2 + k_\perp^2) \quad (4)$$

then,

$$k_\parallel = [(2m / \hbar^2 * E_K)]^{1/2} \sin\theta \quad (5)$$

where, θ is the emission angle measured with respect to the surface normal, and

$$k_\perp = [(2m/\hbar^2 * E_K \cos^2\theta + V_o)]^{1/2} \quad (6)$$

where, V_o is the inner potential, and we refer the interested reader to a review which discusses the details of the ARPES technique extensively [17].

1.6 Complementary Techniques

1.6.1 Inverse photoelectron spectroscopy

In inverse photoelectron spectroscopy [10], one carries out the inverse experiment of photoelectron spectroscopy to study the unoccupied states of a material. A mono-energetic beam of electrons is incident on a material. It occupies an available electronic state as its final state, which is not occupied in the initial state, and emits a photon. By scanning the incident electron energy and measuring detected photons at a fixed photon energy, it is possible to map out the unoccupied density of states of a material. In this mode, it is called bremsstrahlung isochromat spectroscopy (BIS).

1.6.2 X-ray absorption spectroscopy

X-ray absorption spectroscopy (XAS) is a measurement of the X-rays absorbed by a material as a function of the incident X-ray photon energy. In particular, the intensity of X-rays absorbed by a solid undergoes a sharp increase when the incident X-ray photon energy is tuned across a core-level threshold energy [11]. The intensity is directly proportional to

$$I_{XAS} \propto |\langle \Theta_f | \underline{\hat{\mathbf{e}}} \cdot \mathbf{r} | \Theta_i \rangle|^2 \, \delta(E_f - E_i - h\nu) \quad (7)$$

where Θ_i, Θ_f are the initial and final states of the system, and $\underline{\hat{\mathbf{e}}} \cdot \mathbf{r}$ is the dipole operator coupling the initial state with energy E_i to the final state with energy E_f on absorption of an X-ray photon of energy, $h\nu$. The material absorbs a photon and results in exciting an electron to a continuum or an unoccupied state, when the energy $h\nu$ equals $E_f - E_i$. The dipole matrix element approximation indicates that only transitions with $\Delta L = \pm 1$, and which conserve spin $\Delta S = 0$ are allowed transitions. Thus, XAS probes the site selective, element specific, angular momentum projected density of unoccupied states of a material. For soft X-rays (30 – 2000 eV), the quadrupole transition is very weak (usually 100 or more times weaker than the dipole transition) and is often neglected in discussions of soft XAS.

1.6.3 Resonant photoelectron spectroscopy

Resonant photoelectron spectroscopy (RESPES) measures the occupied partial density of states [12], and is thus a complementary technique to XAS. In RESPES, the photon energy is also tuned across a core-level threshold and one measures the valence band photoelectron spectra as a function of the incident photon energy. In this way one can probe the angular momentum projected density of states in the occupied valence band, *e.g.* when the incident photon energy is tuned across the 2p (3d) core level of a 3d transition metal (4f rare-earth) element or compound, the 3d (4f) partial density of states in the valence band can be identified. The process resulting in resonant photoelectron emission involves the absorption of a photon and creation of a core hole (like XAS), and this state undergoes a de-excitation, with the core hole getting filled up and the emission of an electron from the valence band. The remarkable increase in intensity often leading to so-called giant resonances are described by the Fano effect [18]. The experiments of XAS and RESPES are done across particular core-level thresholds and thus necessarily require synchrotron radiation.

1.7 Synchrotron Radiation

Synchrotron radiation [19] is electromagnetic radiation generated by the acceleration of relativistic (near the speed of light) charged particles, *e.g.* electrons, through magnetic fields. The acceleration is first done in a synchrotron, a cyclic particle accelerator in which, the electric field used for accelerating the particles and the magnetic field used for turning the particles for circulation, are synchronized to the particle beam. The high speed electron beam achieves a final energy that is in the GeV (giga-electron-volt) range, and it is stored in the UHV ring in a closed loop. Since the electrons are forced to travel in a closed loop by strong applied magnetic fields, they undergo acceleration and thus emit electro-magnetic radiation which includes frequencies from radio waves, infra-red, visible, ultraviolet and X-rays. The synchrotron radiation sources are the brightest known sources of X-rays, which can be linearly or circularly polarized. The electromagnetic radiation can be further intensified by using insertion devices, called wigglers or undulators (composed of an array of north and south pole magnets). The storage ring has openings through which the radiation exits the storage ring and which are subsequently monochromatized using grating- or crystal-monochromator to obtain a specific energy X-ray beam. Figure 7 shows a typical layout of the setup for the HAXPES experiment, based on a crystal mono-chromator with X-ray optics, and the inserted photograph at the right-upper corner shows the apparatus for Hard X-ray ($6-8$ keV) Photoelectron Spectroscopy (HAXPES) [20]. Several recent HAXPES studies have now established that photoelectron spectroscopy can indeed probe the bulk sensitive electronic structure of solids in a reliable way [20]. The beamline X-ray optics is necessary for obtaining a controlled beam size of a few tenth of microns, which is focussed, collimated and delivers a high photon flux.

Typical applications of synchrotron radiation are :

Diffraction, single crystalline and powder, of inorganic and organic materials, biomaterials (including proteins), *etc.*

X-ray scattering : small angle, magnetic, inelastic, *etc.*

Tomography and imaging

Photolithography

X-ray absorption

X-ray photoelectron spectroscopy

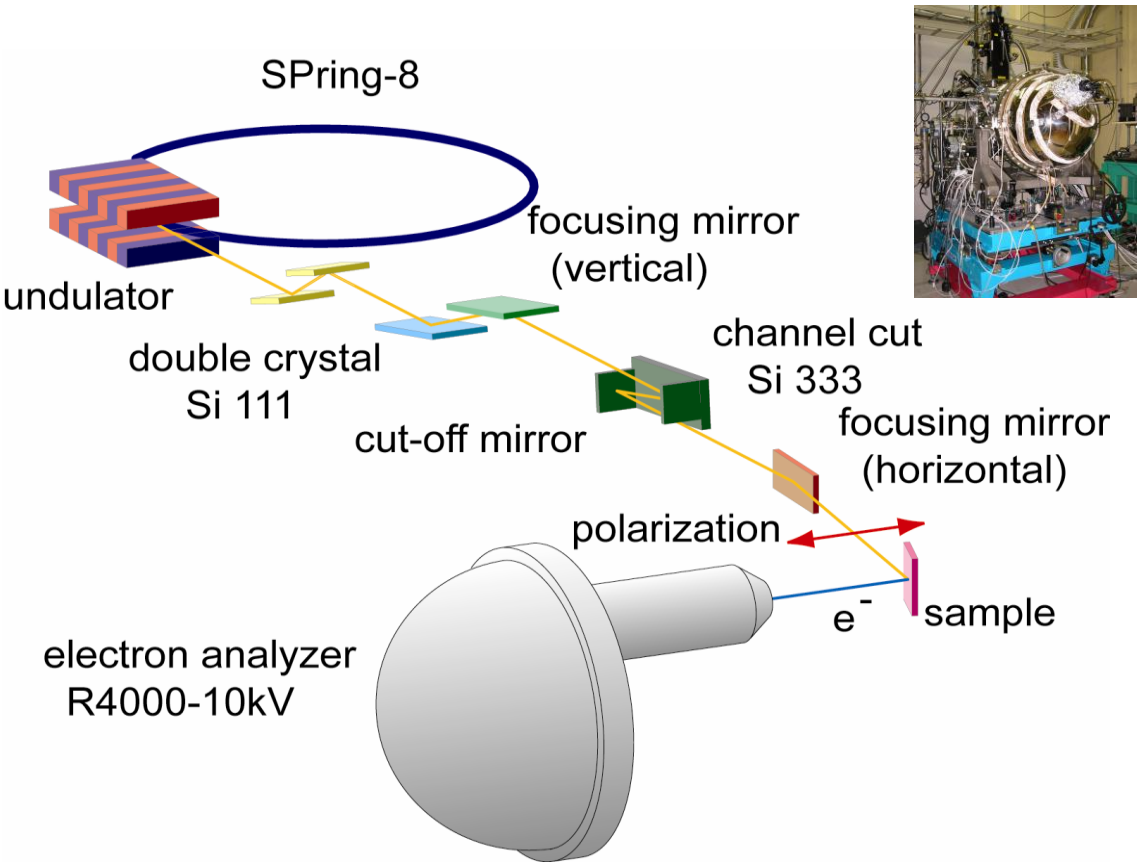

Figure 7. Typical layout of the setup for the HAXPES experiment. Inserted photograph at the right-upper corner shows the HAXPES apparatus installed in the experimental hutch of BL29XU.

The ability of synchrotron radiation sources to provide highly focused, high photon fluxes over a wide energy range, which can be monochromatized to obtain a tunable photon source, plays a major role in present day spectroscopy. In the last 10 years since the advent of the third generation synchrotron sources, typically, a 100- to 1000-times increase in photon flux, with an energy and spatial resolution better than laboratory sources has revolutionized spectroscopy, and also scattering, diffraction and imaging techniques.

2. Experimental

2.1 Brief description of the 27m-long undulator beamline BL19LXU

2.1.1 Overview

RIKEN SR Physics beamline, BL19LXU, has been constructed in 2000 [21] to utilize a high-brilliance X-ray beam generated from a 27m-long undulator [22]. In the optics hutch, a Si(111) double crystal monochromator and a double mirror system have been installed with standard transport-channel components in 2000 and 2004, respectively. Three experimental hutches of EH1 to EH3 are connected to the optics hutch in tandem as shown in Figure 8.

The commissioning of beamline has been started in October 2000. In the spring of 2001, the extension of another experimental hutch EH4, which is located at an extension building of annex West around 130 m from the source (see Figure 8), has been completed. The research and developments have been focused on the experiments which require high-brilliance X-ray beam, such as X-ray free electron laser applications.

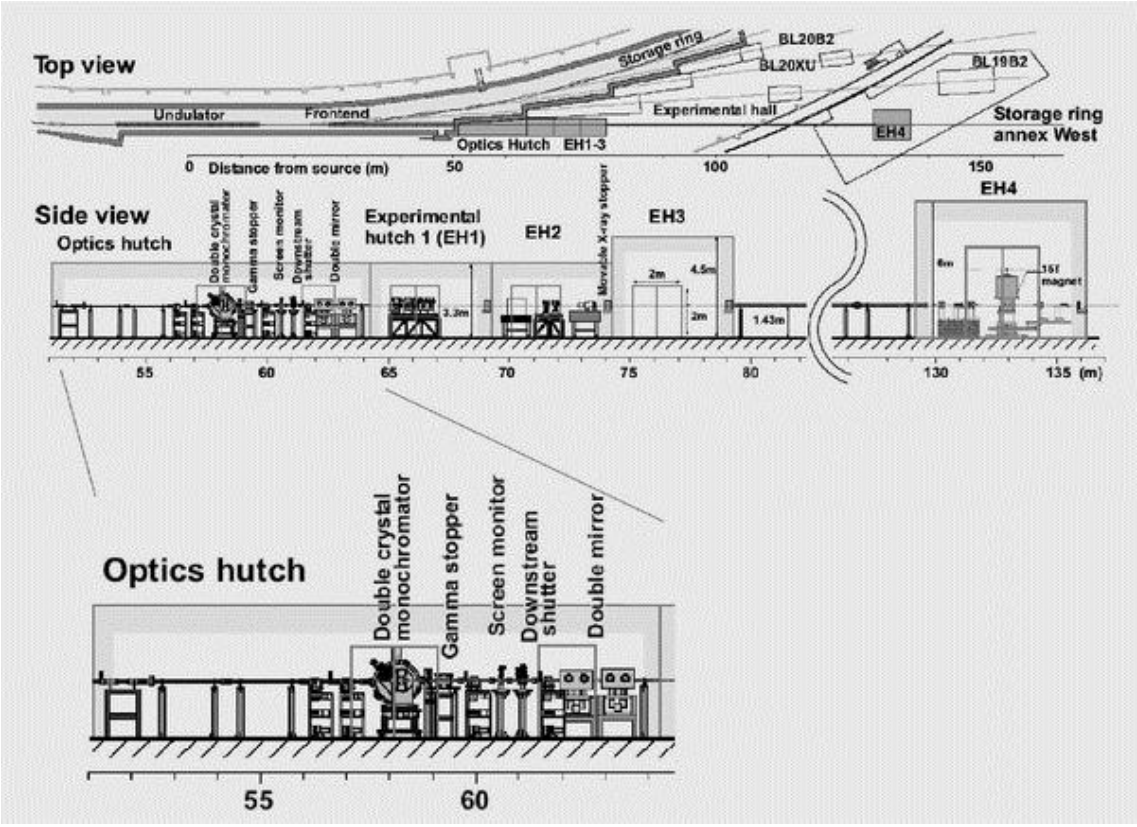

Figure 8. Layout of RIKEN SR Physics beamline BL19LXU

2.1.2 Light source and optics

BL19LXU is mainly characterized by the long undulator [22] shown in Fig. 9. The total length of the undulator magnet is 25 m with a magnetic period length of 32 mm (781 periods) and a maximum K value of 1.77 at 12 mm gap. A photon energy range from 7.2 to 18 keV is covered by the fundamental radiation of the undulator. Although the total radiation power reaches 35 kW at a maximum, most of the off-axis power is removed in the front-end (FE) section [23]. The FE-slit picks up the on-axis portion of the undulator radiation with a power of about 500 W. The radiation passing through the FE-section is monochromatized by a SPring-8 standard type Si(111) double crystal monochromator (DCM). As the first crystal of DCM receives the undulator power, the liquid-nitrogen based cryogenic cooling system is installed to reduce the heat-load on the first crystal. In order to stabilize the throughput of DCM, the first crystal angle can be controlled with MOSTAB feedback system [24, 25]. The resultant energy resolution of X-ray beam is about 10^{-4}. A double mirror system can optionally be used to obtain a focused beam and to remove the higher harmonics passing through the DCM. The locations of first and second mirrors are 46.80 m and 47.95 m from the source, respectively. The Pt-coated mirrors with a length of 400 mm can be bent mechanically with turning of the angle and the shift in height. Available photon energy range and the flux at experimental hutches are summarized in Table 1.

Figure 9. Photograph of 27m-long undulator

Table 1. SR beam parameters at a sample position

Photon energy range	7.2～18 keV (1st), 22～37 keV (3rd) (Si(111))
Photon energy resolution	～1 x 10^{-4}
Photon flux	～2 x 10^{14} photons/s (@ 14 keV)
Beam size (FWHM)	0.8 (V) x 1.5 (H) mm^2 (EH2) (without mirror)

2.1.3 Experimental stations and the equipments

Four experimental hutches (EH1 - 4) are located as described above : A series of experimental hutches of EH1 to 3 is directly attached to the optics hutch in the storage ring building, and EH4 is located in the annex West. The X-rays are guided from EH3 to EH4 through 51m-long Pb-shielded vacuum ducts with the ICF152 conflate-flanges. Vacuum ducts can be optionally attached in EH1-3, when an experiment is carried out in EH2, 3 and 4.

Beamline users should bring their own equipments into the experimental hutches in principle. The details of the experimental hutches are shown below.

- EH1

  EH1 has a dimension of 5 (W) x 3.3 (D) x 3.3 (H) m^3. An air conditioner stabilizes room temperature within 0.1 K fluctuation. In this hutch, fundamental studies have mainly been conducted : such as X-ray correlation, nonlinear optical process, hard X-ray photoelectron spectroscopy, photo-desorption process on the surface and so on.

- EH2

  EH2 is equipped with a femtosecond pulsed laser system [26]. To avoid chirping of the laser pulse, the whole laser system is placed inside the hutch. Synchronization of the laser and SR X-ray pulses is achieved, with a precision of 5 ps, to conduct laser-pump SR-probe time-resolved experiments. For example, a precise dif-fractometer has been installed for picoseconds time-resolved X-ray diffraction studies of lattice dynamics in semiconductors and photochromic crystals, and of the crystallization process in phase change materials, and so on.

- EH3

  Until FY2014, EH3 was the open hutch, located at 77 m from the source, with a dimension of 5 (W) x 3.3 (D) x 4.5 (H) m^3. Very recently, a K-B mirror system is set permanently in the upstream area. Users can install their large instruments such as vacuum chambers or cryostats by using a chain block. Up to now, various new type of experiments have been conducted, such as a scanning tunneling microscope with SR, an X-ray interferometer, an ordinary HAXPES experiment, and also fundamental experiments toward X-ray free electron laser applications.

- EH4

  The hutch EH4 with a large dimension of 7 (W) x 6 (D) x 6 (H) m^3 is located at annex West around 130 m from the source. EH4 is equipped with a multi-circle diffractometer mounting a 15 T super conducting magnet, as well as a pulsed magnet, for studying X-ray magnetic scattering under intense magnetic field and extremely low temperature. A set of K-B mirror has been installed for the development of nano-focusing technique to obtain a beam size of 100 nm in practical application [27].

Equipments available for users are listed below : (1) Timing signal supply ; The 508.58 MHz radio frequency (RF) signal of the storage ring is provided as a trigger of timing experiments. (2) Optical benches ; Optical benches are prepared for various experiments. The dimension is 1.0 m by 2.0 m for one bench, 1.0 m by 1.2 m for two. (3) X-ray detectors ; Ion chambers with a length of 3.3 cm and 14 cm are prepared to monitor the incident X-ray beam intensity. Scintillation counters and PIN photodiodes are also available to monitor the scattered X-ray intensity. (4) Motor control system ; A pulse motor remote control system is available to use stepper motors inside experimental hutches. (5) Electronic circuit for signal processing ; Electronic circuits such as a counter,

a logic controller, a current amplifier, and so on, together with NIM power supplies are prepared for signal processing for various applications.

2.2 HAXPES apparatus and some miscellaneous components for the BL practice

The HAXPES apparatus mainly consists of the hemispherical electron energy analyzer R4000-10kV (VG SCIENTA) mounted on an ultra-high-vacuum system. In addition to the analyzer, a sample manipulator with a motorized XYZΘ stage, a flow-type He cryostat for sample cooling, and two turbomolecular pumps are equipped on the main chamber. This analysis system together with load-lock and preparation chambers are mounted on position-adjustable stages. The vacuum of the main chamber is of the order of 10^{-8} Pa, and the lowest sample temperature that can be achieved is about 30 K. Figure 10 shows a photograph of HAXPES apparatus for the present BL practice. Details for the apparatus are described in Ref. [28, 29].

In the practical course, the HAXPES apparatus is installed in EH3 together with some additional optical components (a high-resolution Si(444) channel-cut monochromator and a horizontal refocusing mirror system) and also some diagnostic devices (some ion chambers and an avalanche photodiode). Optical-laser beam generated from the femtosecond laser system installed in EH2 will be guided to the target material via the laser transport channel. Timing between the optical-laser and SR X-ray pulses can be monitored by using a fast avalanche photodiode. Delay between these two pulses can be adjusted using a digital delay unit.

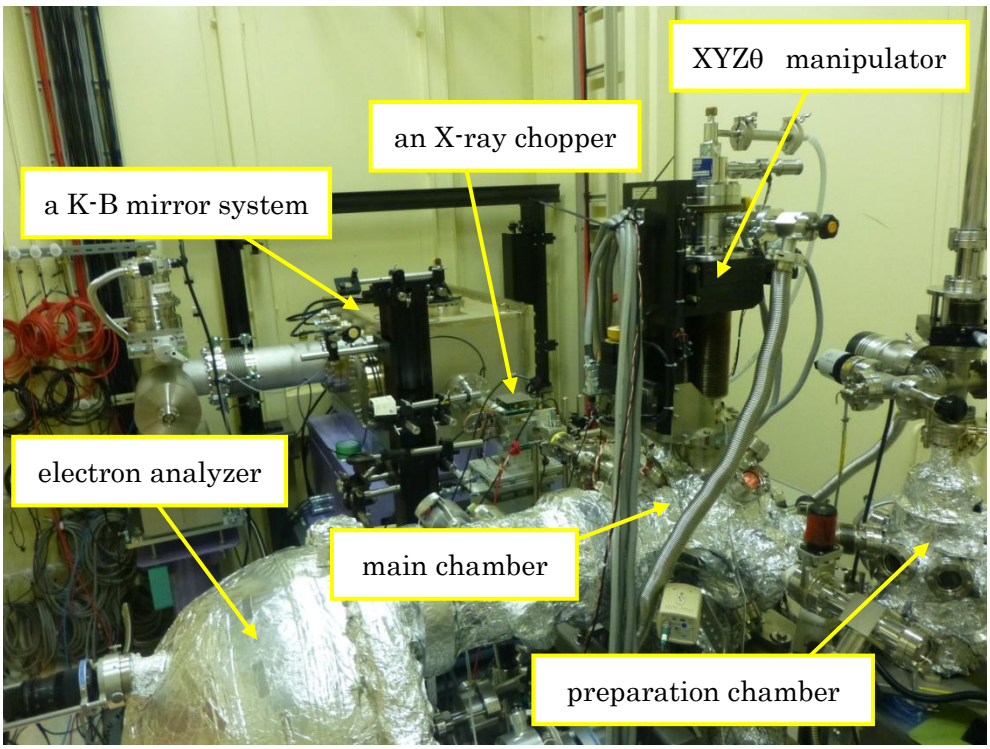

Figure 10. Photograph of a K-B mirror system, an X-ray chopper, and the HAXPES apparatus installed in the experimental hutch EH3 of BL19LXU, SPring-8.

3. Experimental procedure

In this practical course, participants will be asked to proceed the steps which are briefly described in the following subsections.

3.1 Preparation of SR-beam

We will basically use the X-ray beam of about 7.94 keV. First, we will adjust the DCM, which provides us the intense X-ray beam of $\Delta E/E \sim 1.6 \times 10^{-4}$ ($\Delta E \sim 1.3$ eV), by looking at the rocking curve. Reflectivity as a function of angle will be measured by using an ion chamber (IC). We will also adjust the position of the transport-channel (TC) slits by monitoring the intensity of X-ray beam passing through the TC-slit. The parameter of an insertion device (ID), *e.g.* gap, will be set to provide the maximum output by monitoring the readout of IC. After adjustments of the ID, DCM and TC-slit, we will adjust the Si(444) channel-cut monochromator, which will be used to provide the high-resolution X-ray beam of $\Delta E \sim 60$ meV. This high-resolution X-ray beam will be horizontally and vertically focused using a couple of refocusing mirrors. Then we will see the X-ray beam position at the entrance of the HAXPES apparatus by using a burn-paper.

3.2 Sample preparation

It is the custom for the ultra-high vacuum (UHV) apparatus, which is used for spectroscopic study, to put the sample into the UHV condition with special care. In the case of our HAXPES apparatus, first we usually install the sample to the load-lock chamber ($< 10^{-5}$ Pa), then we transfer it into the preparation chamber ($< 5 \times 10^{-8}$ Pa) by using the transfer-rod. In the preparation chamber, we sometimes fracture the sample under the UHV condition in order to get a clean surface. Finally, we transfer the sample into the main chamber ($\sim 2 \times 10^{-8}$ Pa) by using the transfer-rod.

3.3 Adjustment of the apparatus

In order to adjust the apparatus to its optimum condition, we will introduce the X-ray beam into the main chamber. We will monitor the X-ray beam at the sample position by using the fluorescent material painted on the Cu holder. We will view the fluorescence by using the CCD cameras and a TV-monitor. After marking the beam position on the monitor, we will move the Z-axis of XYZΘ manipulator to the position of standard sample, *i.e.* Au coated plate. We will measure the Au 4f photoelectron spectra, and adjust the sample XYZΘ-manipulator and the height of the apparatus so as to maximize the counting rate of the Au 4f photoelectron signals.

3.4 Calibration of the electron analyzer

We are using the hemispherical electron-energy analyzer R4000-10kV (VG-SCIENTA). Pass-energy of 200 or 500 eV is usually used for our HAXPES measurements.

The control software, especially for the lens parameter, is well prepared, but sometimes there exists an undesired energy offset for each pass-energy when we measure the kinetic energy spectrum of photoelectrons emitted from the sample. Thus we need to calibrate the analyzer to determine this energy offset. It will be performed by measuring the photo-electron spectra from the standard Au sample.

3.5 Measurements of electron spectra of today's sample

We will measure some electron spectra of the today's sample with wide-energy range, narrow-energy range for each core-level, near the valence-band region and also some KLL and/or LMM Auger transitions.

3.6 Adjustments of the X-ray chopper and the timing between pump- and probe-pulses

In order to establish the pump-probe measurement scheme, the X-ray chopper will be installed into the SR-beam axis and aligned so as to select the X-ray bunch with the repetition rate of about 1 kHz. We can monitor the signal of chopped X-ray beam using the fast photodiode and oscilloscope. By using the fast photodiode, we will adjust the timing between the optical pump-laser and the SR probe X-rays. The delay time between pump- and probe-pulses will be adjusted by using the digital delay unit.

3.7 Introduction of optical pump-laser

After the adjustment of the X-ray chopper, we will introduce the optical-laser beam into the main chamber. The position of the laser beam will be adjusted to the marked position determined in subsection of 3.3. Participants are asked to wear goggles for their safety.

3.8 Observation of photoinduced carrier dynamics

First we will measure the Si 1s HAXPES spectrum, as an undistorted spectrum, using the chopped X-ray beam without pump-laser irradiation. After that, we will measure few spectra as a function of the delay time between pump- and probe-pulses. We will be noticed that the kinetic energy of photoelectrons emitted from the Si 1s core-level will be shifted by the pump-laser irradiation.

4. Discussion for the available time-resolved HAXPES.

Time-resolved spectroscopy is the special method to study the dynamic processes in materials or chemical compounds by means of spectroscopic techniques. For the photoelectron spectroscopy, transient processes in condensed matter are typically recorded as photoelectron spectra by using probe-pulse after excitation by pump-laser irradiation. In a typical experiment, both of the photon-pulses for pump and probe are ultra-short pulsed-beam. Temporal evolution of the photoelectron spectra as a function of delay-time between pump- and probe-pulses gives us dynamic information on the transient electronic

structure of condensed matter.

Since 2012, we have been making efforts to realize time-resolved HAXPES to study the ultrafast electron dynamics for materials science. Recently, we have developed a single-shot CCD-based data acquisition system for time-resolved X-ray photoelectron spectroscopy at an X-ray free electron laser facility [30]. We have successfully demonstrated the capability of the system by measuring the core-level HAXPES spectra at SACLA XFEL facility and studied the time-resolved space-charge effects on the Ti 1s and V 1s core-level photoelectron spectra [31,32].

The time-structure of X-ray beam is determined by the electron bunches in the storage ring. The each electron bunch has the pulse width of about 40 ps with full width at half maximum (FWHM), with a repetition rate up to 509 MHz. The repetition rate can be selected by the operational mode of the storage ring with preference filling pattern. Typical filling pattern is represented in Figure 11. In the BL practice, the filling pattern operated is H-mode, which is suitable for pump-probe type time-resolved HAXPES. Typical parameters for the filling pattern shown in Figure 11 are summarized in Table 2.

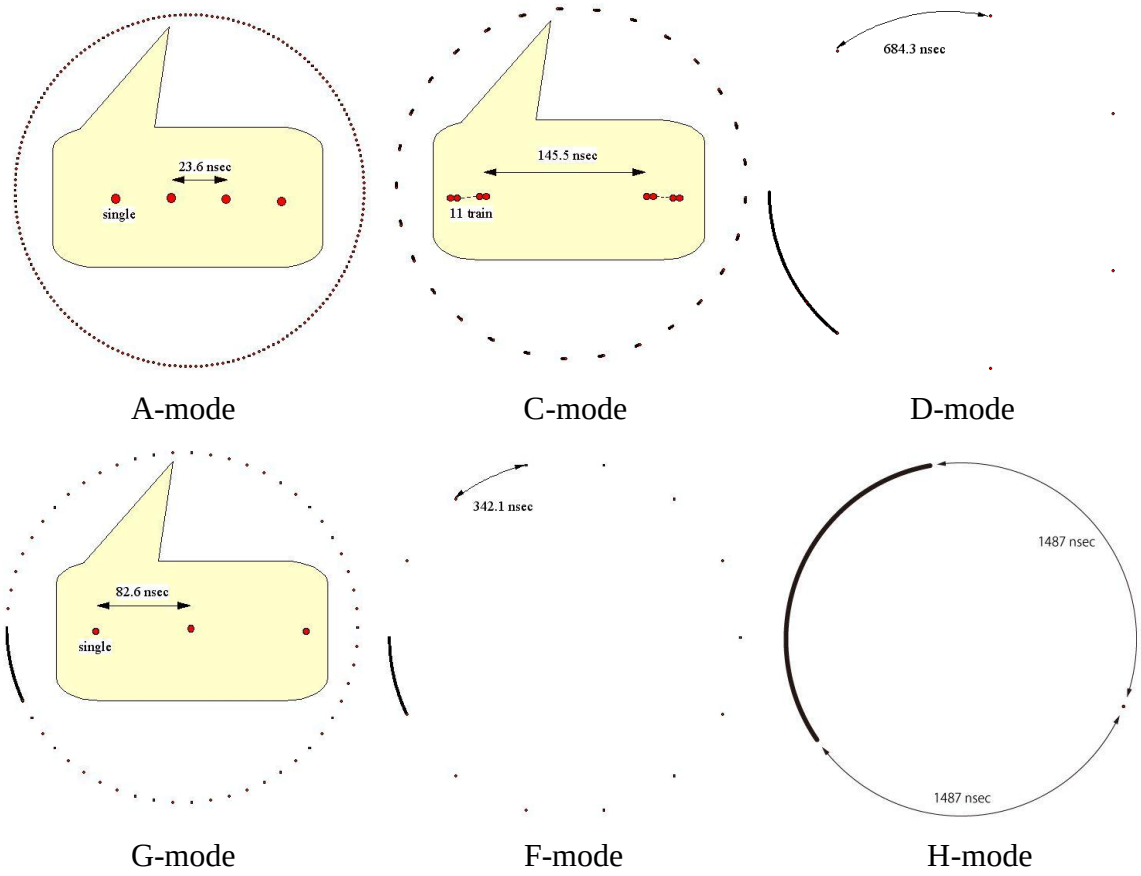

Figure 11. Examples of the filling patterns of electron bunches in the storage ring.

Table 2. Typical parameters for several bunch operational mode

Mode	Bunch mode	Bunch interval	Total current	Single bunch current	Beam injection interval
A-mode	203 bunches	23.6 ns	100 mA		30 s
C-mode	11 bunch train x 84	145.5 ns (165.2 ns period)			40 s
D-mode	1/7-filling + 5 bunches	684.3 ns		3.0 mA	20 s
F-mode	1/14-filling + 12 bunches	342 ns		1.6 mA	20 s
G-mode	4/58-filling + 53 bunches	83 ns		1.0 mA	20 s
H-mode	11/29-filling + 1 bunch	1486 ns		5 mA ～	40 s

The femtosecond laser system is composed of the mode-locked laser oscillator, and a regenerative amplifier to produce laser pulses with a pulse-duration of about 130 fs and a pulse energy of about 1 mJ/pulse. The laser pulses are synchronized with the RF master oscillator of the storage ring which controls the acceleration timing of the electron bunches [26, 33, 34]. The synchronization and timing control system are depicted in Figure 12 together with the present experimental setup.

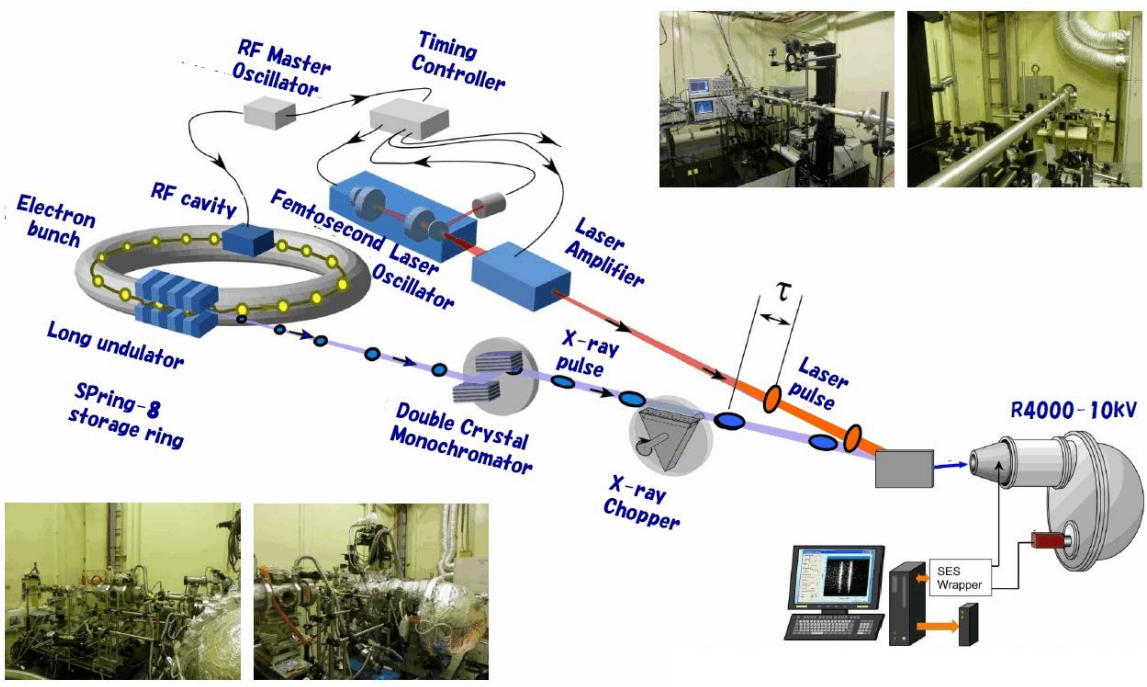

Figure 12. Experimental setup for the time-resolved HAXPES at BL19LXU

In order to realize time-resolved HAXPES, it is important to achieve the condition of same repetition rates for both the optical pump-laser and X-ray probe-pulse. We are usually using the X-ray chopper to chop the 208 kHz X-ray pulses in H-mode to match with the repetition rate of the pump-laser, *e.g.* 1 kHz typically. This will enable us to accomplish a complete pump-probe configuration scheme for the time-resolved HAXPES experiment.

In Figure 13, we show a time chart of the laser and the SR pulses for the pump-probe measurement. In the figure, the time chart for the SR pulses are represented for D-mode (5-bunches + 1/7 filling). The SR pulse selected by the X-ray chopper is generated from a high-current electron bunch (3 mA). By adjusting the time-delay τ, we can measure the temporal evolution of the transient electronic structure as a movie with the time resolution of about 40 ps (pulse width of the X-ray SR).

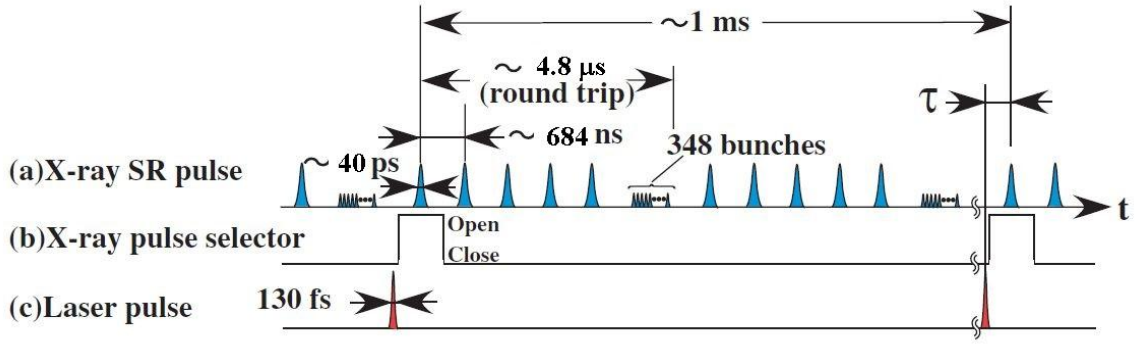

Figure 13. Time chart of the pulsed laser, X-ray SR, and the gate of an X-ray pulse selector, *i.e.* the X-ray chopper, for a snapshot measurement with a time-delay of τ [33].

In the BL practice, we will see the recent results for the time-resolved HAXPES experiments to investigate the ultrafast lead-lag electron dynamics of space-charge effects on the core-level HAXPES spectra [31,32] and also the results of the observation of photoinduced carrier dynamics at the SiO_2/Si and the Si/SiO_2 interfaces [35].

References

[1] S.Hüfner, Photoelectron spectroscopy : Principles and Applications, 3rd edition (Springer-Verlag, Berlin, Heidelberg, 2003).

[2] H.Hertz, Ann. Physik **267**, 983 (1887).

[3] A.Einstein, Ann. Physik **17**, 132 (1905) ; Trans. Into English, Am. J. Phys. Vol.33, n.5 (1965).

[4] K.Siegbahn, C.Nordling, R.Fahlman, R.Nordberg, K.Hamrin, J.Hedman, G.Johansson,

T.Bergmark, S.-E.Karlsson, I.Lindgren, B.Lindberg : ESCA-Atomic, Molecular and Solid State Structure Studied by Means of Electron Spectroscopy, Nova Acta Regiae Soc. Sci., Upsaliensis, Ser. IV, Vol. 20, 1967.

[5] D.Briggs and M.P.Seah, Practical Surface Analysis by Auger and X-ray Photoelectron Spectroscopy (John Wiley and Sons, New Jersey, 1983).

[6] H.Ibach, Electron Spectroscopy for Surface Analysis, Topics in Current Physics Vol.4 (Springer, Berlin, Heidelberg, 1977).

[7] S.Tanuma, C.J.Powell and D.R.Penn, J. Vac. Sci. Techn. A**8**, 2213 (1990).

[8] National Institute of Standards and Technology (NIST) Photoelectron Spectroscopy Database, http://srdata.nist.gov/xps/.

[9] A.Beiser, Concepts of Modern Physics, 6th edition (McGraw-Hill Science, New York, 2002).

[10] V.Dose, Appl. Phys. **14**, 117 (1977) ; M.Donath, Surf. Sci. Rep. **20**, 251 (1994).

[11] F.De Groot, Chem. Rev. **101**, 1779–1808 (2001).

[12] J.W.Allen, in Synchrotron Radiation Research: Advances in Surface and Interface Science, edited by R. Z. Bachrach _Plenum, New York, 1992, p. 253–323.

[13] J.J.Yeh and I.Lindau, At. Data Nucl. Data Tables **32**, 1 (1985).

[14] G.Hollinger and F.J.Himpsel, Appl. Phys. Lett. **44**, 93 (1984) ; M.Shioji, T.Shiraishi, K.Takahashi, H.Nohira, K.Azuma, Y.Nakata, Y.Takata, S.Shin, K.Kobayashi, and T.Hattori, Appl. Phys. Lett. **84**, 3756 (2004).

[15] S.Doniach and M.Sunjić , J. Phys. C**3**, 285 (1970).

[16] T.Kiss, T.Shimojima, K.Ishizaka, A.Chainani, T.Togashi, T.Kanai, X.-Y.Wang, C.-T. Chen, S.Watanabe and S.Shin, Rev. Sci. Instrum. **79**, 023106 (2008).

[17] E.W.Plummer and W.Eberhardt, Adv. Chem. Phys. **49**, 533 (1982).

[18] U.Fano, Phys. Rev. **124**, 1866 (1961).

[19] Handbook on Synchrotron Radiation, Volume 1a, Ed. Ernst-Eckhard Koch, North Holland, 1983.

[20] Y.Takata, in Very High Resolution Photoelectron Spectroscopy, Ed. S. Hüfner, p. 373 (Springer, Berlin, Heidelberg, 2006) ; and references therein.

[21] M.Yabashi, T.Mochizuki, H.Yamazaki, S.Goto, H.Ohashi, K.Takeshita, T.Ohata, T.Matsushita, K.Tamasaku, Y.Tanaka, and T.Ishikawa, Nucl. Instrum. Methods A**467/468**, 678-681 (2001).

[22] T.Hara, M.Yabashi, T.Tanaka, T.Bizen, S.Goto, X.Marechal, T.Seike, K.Tamasaku, T.Ishikawa, and H.Kitamura, Rev. Sci. Instrum. **73**, 1125-1128 (2002).

[23] S.Takahashi, H.Aoyagi, T.Mochizuki, M.Oura, Y.Sakurai, A.Watanabe, and H.Kitamura, Nucl. Instrum. Methods A**467/468**, 758-761 (2001).

[24] T.Kudo, Y.Nishino, T.Hirono, and T.Ishikawa, HOUSHAKO **16**, 173-177 (2003). (*in Japanese*)

[25] T.Kudo and T.Hirono, SPring-8 Info. **13**, 234-238 (2008). (*in Japanese*)

[26] Y.Tanaka, T.Hara, H.Kitamura, and T.Ishikawa, Rev. Sci. Instrum. **71**, 1268-1274

(2000).
[27] H.Yumoto, T.Koyama, K.Hirata, K.Kawano, G.Ueno, A.Nisawa, T.Hikima, S.Takeshita, H.Ohsumi, K.Ito, Y.Tanaka, T.Arima, H.Ohashi, M.Yamamoto, and S.Goto, AIP Conf. Proc. **1365**, 200-203 (2011)
[28] Y.Takata, M.Yabashi, K.Tamasaku, Y.Nishino, D.Miwa, T.Ishikawa, E.Ikenaga, K.Horiba, S.Shin, M.Arita, K.Shimada, H.Namatame, M.Taniguchi, H.Nohira, T.Hattori, S.Södergren, B.Wannberg, and K.Kobayashi, Nucl. Instrum. Methods A**547**, 50-55 (2005).
[29] Y.Takata, K.Horiba, M.Matsunami, S.Shin, M.Yabashi, K.Tamasaku, Y.Nishino, D.Miwa, T.Ishikawa, E.Ikenaga, K.Kobayashi, M.Arita, K.Shimada, H.Namatame, M.Taniguchi, H.Nohira, T.Hattori, S. Södergren, and B.Wannberg, AIP Conf. Proc. **879**, 1597-1602 (2007).
[30] M.Oura, T.Wagai, A.Chainani, J.Miyawaki, H.Sato, M.Matsunami, R.Eguchi, T.Kiss, T.Yamaguchi, Y.Nakatani, T.Togashi, T.Katayama, K.Ogawa, M.Yabashi, Y.Tanaka, Y.Kohmura, K.Tamasaku, S.Shin, and T.Ishikawa, J. Synchrotron Rad. **21**, 183-192 (2014).
[31] L.-P.Oloff, M.Oura, K.Rossnagel, A.Chainani, M.Matsunami, R.Eguchi, T.Kiss, Y.Nakatani, T.Yamaguchi, J.Miyawaki, M.Taguchi, K.Yamagami, T.Togashi, T.Katayama, K.Ogawa, M.Yabashi, and T.Ishikawa, New J. Phys. **16**, 123045 (2014).
[32] M.Oura, L.-P.Oloff, A.Chainani, K.Rossnagel, M.Matsunami, R.Eguchi, T.Kiss, T.Yamaguchi, Y.Nakatani, J.Miyawaki, K.Yamagami, M.Taguchi, T.Togashi, T.Katayama, K.Ogawa, M.Yabashi, T.Gejo, K.Myojin, K.Tamasaku, Y.Tanaka, T.Ebihara, and T.Ishikawa, Trans. Mat. Res. Soc. Jpn. **39**, 469-473 (2014).
[33] Y.Tanaka, Y.Fukuyama, N.Yasuda, J.Kim, H.Murayama, S.Kohara, H.Osawa, T.Nakagawa, S.Kimura, K.Kato, F.Yoshida, H.Kamioka, Y.Moritomo, T.Matsunaga, R.Kojima, N.Yamada, K.Toriumi, T.Oshima, H.Tanaka, and M.Takata, Jpn. J. Appl. Phys. **48**, 03A001 (2009).
[34] N.Yasuda, Y.Fukuyama, S.Kimura, K.Ito, Y.Tanaka, H.Osawa, T.Matsunaga, R.Kojima, K.Hisada, A.Tsuchino, M.Birukawa, N.Yamada, K.Sekiguchi, K.Fujiie, O.Kawakubo, and M.Takata, Rev. Sci. Instrum. **84**, 063902 (2013).
[35] M.Oura *et al.*, to be published.